The Electronic Structure of Mixed Self-Assembled Monolayers

Ferdinand Rissner,[†] David A. Egger,[†] Lorenz Romaner,[‡,†] Georg Heimel,[§] and Egbert Zojer[†,*]

[†]Institute of Solid State Physics, Graz University of Technology, Petersgasse 16, 8010 Graz, Austria, [‡]Chair of Atomistic Modelling and Design of Materials, University of Leoben, Franz-Josef-Strasse 18, 8700 Leoben, Austria, and [§]Institut für Physik, Humboldt-Universität zu Berlin, Brook-Taylor-Strasse 6, 12489 Berlin, Germany

ABSTRACT The electronic structure of mixed self-assembled monolayers (SAMs) on Au(111) surfaces is modeled using slab-type density-functional theory calculations. The studied molecules have a dipolar character induced by polar and electron donating or accepting tail-group substituents. The resulting electronic structure of mixed layers is found to differ qualitatively from a simple superposition of those of the respective pure layers. Specifically, the positions of the frontier electronic states are shifted relative to the metal Fermi level, with the sign and magnitude of that shift depending on the dipole moment of the molecules and the mixing ratio in the film. This appears counterintuitive considering previous investigations, in which it has been shown that, for densely packed layers, tail-group substituents have no impact on the interfacial energy-level alignment. The seeming contradiction can be lifted by considering the local electrostatic interactions within the films in both mixed and homogeneous monolayers. Beyond that, we show that mixed SAMs provide an efficient tool for continuously tuning substrate work functions over a range that far exceeds that accessible by merely changing the coverage of homogeneous layers, with the net effect depending linearly on the mixing ratio in agreement with recent experimental findings.

KEYWORDS: self-assembled monolayer · metal−organic interface · quantum-mechanical modeling · band-structure calculation · mixed monolayer · heterogeneous surfaces · intermolecular interactions

Covalently bonded self-assembled monolayers (SAMs)[1−3] on noble metals are of ever increasing importance[4,5] for a variety of applications.[6−9] Their electronic properties are exploited in organic (opto)electronic devices to tune electrode properties, which can lead to a significant improvement of device performance.[8,10−13] In particular, the alignment of the frontier energy levels in the organic semiconductor with the Fermi level of the electrode needs to be optimized.[14−16] In this context, the effective work function, Φ, of the electrode is the single most important parameter, which needs to be adjusted through the employment of suitable SAMs. A key quantity of interest is, therefore, the SAM-induced work-function modification, $\Delta\Phi$.

Besides using SAMs for "mere" surface modification, in the quest for ultimate miniaturization, the molecular monolayer itself[17−20] or even individual molecules[21−28] can be used as the functional entity of a device. For such applications, the *alignment between the SAM and the metal states* is of key importance, as the positions of the highest occupied and lowest unoccupied π-states in the SAM relative to the Fermi level of the electrodes determine the tunneling barriers for hole and electron transport.

Great effort has been made to understand and control the electronic properties of SAM-modified surfaces, both experimentally[29,30] and through computational modeling.[31−35] In-depth knowledge on the impact of the docking chemistry,[36,37] the molecular polarizability,[38] depolarization effects,[39−43] and (dipolar) donor- and acceptor substituents[31,44] has been seen to be of uttermost importance for designing molecular structures that lead to SAMs with the desired characteristics.

An alternative approach for tuning SAM properties is to fabricate mixed layers of different functional molecules.[45−51] Following this strategy, Wu *et al.*[52] have shown that, by combining SAMs of alkanethiols and fluorinated alkanethiols, the substrate work function can be adjusted in an almost linear fashion as a function of the mixing ratio. The fabrication of well-ordered mixed layers is an experimental challenge and phase segregation is frequently observed.[47,53−59] While for some applications this can be exploited,[60] mixing at the molecular level is usually desired. One approach to prevent segregation is to intentionally generate defects in a well-ordered homogeneous SAM by electron irradiation or UV light exposure. In this way, a place-exchange reaction can be promoted in which part of the molecules are replaced by another component

*Address correspondence to egbert.zojer@tugraz.at.

Received for review September 10, 2010 and accepted October 13, 2010.

Published online November 3, 2010. 10.1021/nn102360d

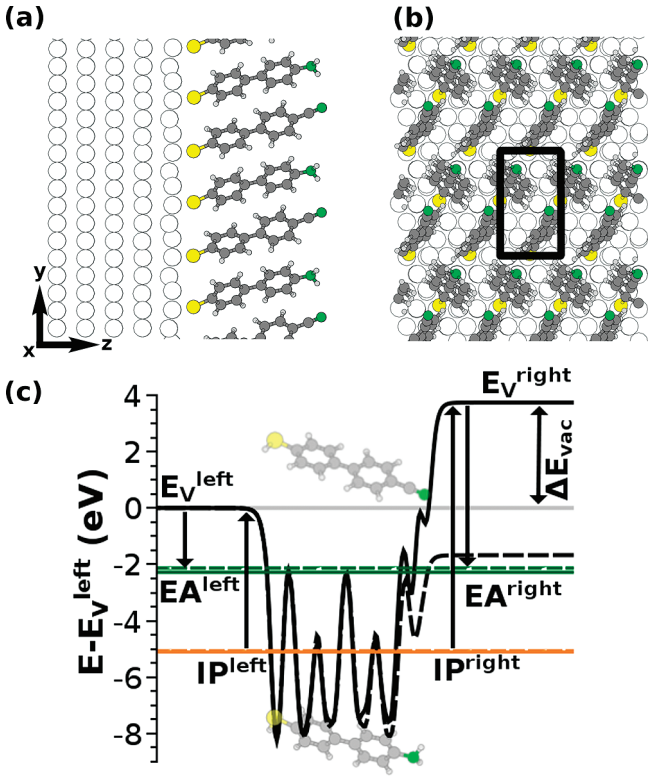

Figure 1. Side (a) and top (b) view of the biphenylthiolate SAM on a five-layer Au(111) slab. In the depicted case, cyano and amino substitutents are mixed in a ratio of 1:1. The Cartesian directions are indicated. The black rectangle marks the $p(\sqrt{3} \times 3)$ surface unit cell and the molecules are packed in a herringbone pattern. (c) *x,y*-averaged electrostatic energy of an electron across a hypothetical free-standing densely packed homogeneous SAM (solid [dashed] line: cyano-[amino-] tail group). Left- and right side vacuum energy (E_v), $\Delta E_{vac} := E_v^{right} - E_v^{left}$, ionization potential (IP), and electron affinity (EA) are indicated.

to obtain a mixed film.[49,61,62] Another strategy to realize mixed SAMs is to attach both functional groups of interest to the same molecule.[55,63−66] Silien *et al.*[51] succeeded in using a network of flat-lying molecules as mask[67] for patterning a binary SAM on the nanoscale and Pace *et al.*[68] have shown that under certain circumstances it is possible to produce crystalline mixed domains. In layers ordered that well, one can exploit the fact that the local electrostatic environment of adsorbed molecules crucially impacts their properties. Such considerations have, for example, been used for explaining the mixing-ratio dependent ultraviolet photoelectron spectroscopy (UPS) results observed for mixed pentacene and perfluoro-pentacene layers.[69] Furthermore, in single-molecule transport experiments the conductivity is distinctly different for isolated molecules and for molecules assembled in a monolayer;[70] such a situation is in some sense reminiscent of a previous computational study[43] in which SAMs at reduced coverage but essentially in their monolayer geometries have been investigated. We are, however, not aware of a computational study that provides a systematic investigation explaining the peculiar properties of a mixed SAM that consists of two different functional molecules. Here, we provide such a study. Specifically, we address the question of how the electronic properties of a molecular layer change when it is patterned on a subnanometer scale. As we will show in the following, the electronic properties of a mixed SAM differ qualitatively from what one might naively derive from the properties of the two neat layers, with each of them consisting of only one of the constituent molecules of the mixed SAM. Resolving that puzzle will require us to disentangle several effects and will reveal electrostatic intermolecular interactions in SAMs as the key issue. To comprehend our observations on mixed monolayers, it is both instructive and revealing to contrast these findings against the properties of homogeneous monolayers.

The System. For the present study, we chose to investigate biphenylthiolate-based SAMs adsorbed on the Au(111) surface (Figure 1) because such SAMs have been subject to extensive experimental[71−78] and computational[31,36,39,41−44,79] studies. For methyl-substituted biphenylthiolates on the Au(111) surface a $p(\sqrt{3} \times 3)$ unit cell has been suggested,[73,77] which serves as an important input for our calculations. These rely on density-functional theory (DFT) based, slab-type band-structure calculations in which the interface is modeled by five metal layers on top of which the molecules are adsorbed. As shown in Figure 1b, the surface unit cell contains two inequivalent molecules arranged in a herringbone pattern, which is typical for oligophenylenes.[80] For mixing ratios other than 1:1, a multiple of the cell was chosen. The tilt of the molecular backbone with respect to the surface normal changed only moderately between the systems and was in the range of 14−21°. Further details on the applied methodology can be found in the Methods section. The molecules are assumed to bond to the flat metal surface *via* a thiolate group, which will be referred to as the docking group in the following. In this context, it should be mentioned that the actual structure of the Au−thiolate interface is still subject to controversy,[81] but its details do not impact the main conclusions of the present paper.

By substituting the terminal hydrogen atoms of the biphenylthiolates with strong (polar) donor or acceptor groups (the tail groups), the direction and magnitude of the molecular dipole moment can be controlled. Here, we chose amino ($-NH_2$) and cyano ($-CN$) tail groups as they carry intrinsic dipole moments that point in opposite directions and are very strong donors and acceptors, respectively. Figure 1a,b shows the case of a 1:1 mixing ratio of those tail groups. We note that the role of docking and tail group substituents in such SAMs is well understood[36] and that the results of the present article can be expected to be transferable to other chemical groups of similar functionality, that is, polar donor and acceptor substituents. The electronic properties of homogeneous layers of both amino- or

cyano-substituted biphenylthiolate SAMs have been described in the literature and are briefly reviewed here, as they are key to understanding the properties of mixed layers:[42,43] At dense packing, the $-NH_2$ substitution has been predicted to decrease the work function of the Au (111) surface, while $-CN$ tail groups are expected to increase it.[36,44] Additionally, the *a priori* unexpected observation has been made that the substituent (and, thus, the molecular ionization potential) has no impact on the relative alignment of the metal Fermi level and the highest occupied π-states,[44] at least as long as the SAM packing density was sufficiently high.[43] In other words, the energetic distance between the Fermi level and the highest occupied π-states (HOPS), ΔE_{HOPS}, is identical for both SAMs. The same behavior was observed also for more polarizable (*e.g.*, polyene) and less polarizable (*e.g.*, aliphatic) backbones.[38]

This phenomenon can be explained on electrostatic grounds,[33,35] considering that a 2D extended dipole layer divides space into two regions with vacuum levels differing by an energy proportional to the dipole density as dictated by the Helmholtz equation. This is schematically shown in Figure 1c, where the plane-averaged electron electrostatic energy for a (hypothetical) free-standing SAM is shown. The two vacuum-level energies, E_v^{left} and E_v^{right}, differ by an amount ΔE_{vac}. Consequently, also a left- and a right-sided ionization potential, IP^{left} and IP^{right}, and electron affinity, EA^{left} and EA^{right}, need to be defined. They can be approximated by the energetic difference between the highest occupied (lowest unoccupied) states of the SAM and the respective vacuum levels. The tail-group substituents change the potential energy only on "their side" of the monolayer. Moreover, their impact on the potential energy landscape within the SAM is restricted to their immediate vicinity, consistent with the electrostatic properties of a densely packed dipole layer[82] and depolarization effects within the SAM.[39−43,83,84] Therefore, also the eigenstates within the SAM are hardly affected by tail-group substitution.

What eventually determines the alignment between the potential wells of the metal substrate and the SAM are only the left-sided vacuum level of the SAM, the position of the vacuum level above the metal surface, and the bond dipole that results from bonding-induced charge rearrangements.[32,33,37] The latter are largely localized in the docking-group region and on the top Au layers, resulting in the bond dipole being tail group-independent at full coverage.[44] As a consequence, tail-group substitution with a donor- or acceptor group hardly affects ΔE_{HOPS}, the offset between Fermi energy and HOPS.

RESULTS AND DISCUSSION

SAMs Adsorbed on Au(111). Bearing these properties of the homogeneous monolayers in mind, one might expect that also in the mixed system there should be only a single pronounced maximum in the density of states that is derived from the highest occupied states of all constituent molecules. This is, however, not the case as can be seen in Figure 2. There, the calculated density of states projected onto the SAM (PDOS) is shown for the system depicted in Figure 1, namely $-NH_2$ and $-CN$ substituted biphenylthiolates on Au (111) at a mixing ratio of 1:1.

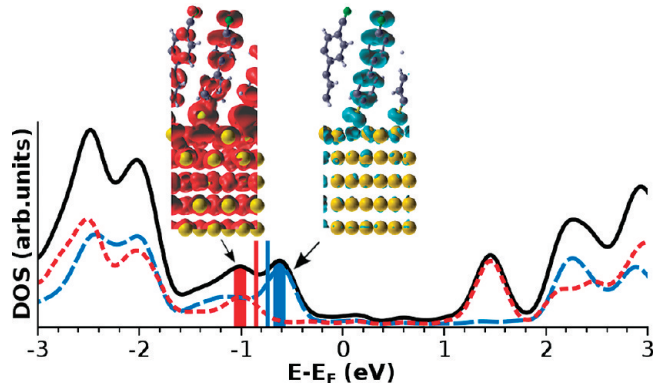

Figure 2. Projected density of states of the mixed SAM on Au(111) with a 1:1 mixing ratio (black line). The dashed blue and dotted red lines show the projections onto only the $-NH_2$ (blue) and $-CN$ (red) substituted subsystems. The insets depict the local densities of states integrated in the energy windows shaded in blue and red, respectively (thick vertical bars). It corresponds to the charge densities in these energy ranges. The thin red and blue vertical lines indicate the positions of the HOPS peak maxima of both components in absence of the respective other fragment (*i.e.*, at half coverage). All curves are aligned to the Fermi energy, E_F.

It displays a pronounced double peak structure between *ca.* -0.5 and -1.5 eV. To understand its origin, we calculated the densities of states projected onto the two subsystems, that is, only on the $-NH_2$ substituted (blue line in Figure 2) and $-CN$ substituted (red line in Figure 2) biphenylthiolates within the mixed SAM. Their comparison clearly shows that the highest peaks belonging to the respective subsystems do not coincide in the mixed monolayer; rather, the highest PDOS peak is localized only on the $-NH_2$ substituted molecules. This can also be inferred from the corresponding local density of states (LDOS) shown as the right inset of Figure 2 which, furthermore, confirms the π-character of the corresponding molecular orbital. The highest peak that also comprises states on $-CN$ substituted molecules is found at 0.4 eV lower energies. From the LDOS plot, those states are confirmed as the HOPS of the $-CN$ substituted sub-system that energetically overlap with the tails of the HOPS peak and a lower-lying state on the $-NH_2$ substituted subsystem. Considering that charge-carrier injection depends exponentially on the barrier height that results from the level alignment, a shift by 0.4 eV is a sizable effect. Moreover, this surprising finding shows that the electronic structure of the mixed SAM qualitatively differs from that of both the $-CN$ and the $-NH_2$ substituted SAMs. There, as discussed in the previous section, the respective HOPS peaks in the homogeneous layers at full coverage are

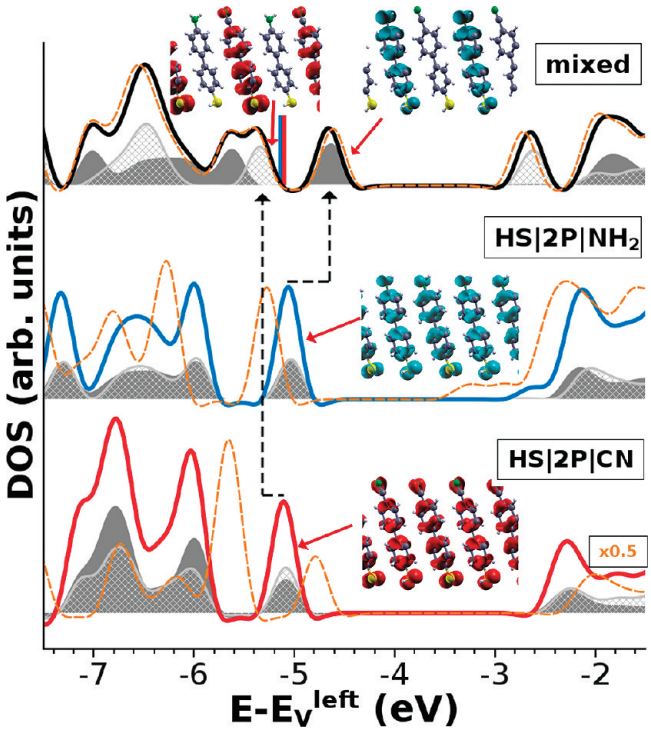

Figure 3. DOS of the free-standing mixed and the respective pristine SAMs (top to bottom). The dark gray filled and light gray crossed areas show the DOS projected onto the two inequivalent components of the respective monolayers separately. The insets show the charge density in real space (LDOS) in energy windows of 0.1 eV around the respective peak maxima. The dashed black arrows indicate the splitting of the HOPS levels in the mixed layer compared to the pure layers. Dashed orange lines show the DOS resulting from nonselfconsistent (nscf) calculations in which no (de)polarization is allowed upon merging the two components. For details see text. In the bottom panel, the nscf-DOS is divided by 2 to save space. The two touching vertical lines in the topmost panel show the HOPS positions for both components in the absence of the respective other fragment in analogy to Figure 2. All curves are aligned at the vacuum energy on the thiol side of the SAM, E_v^{left} (*cf.* Figure 1c).

calculated to be within 0.03 eV (at −0.96 for the $-NH_2$ substituted and −0.99 eV for the −CN substituted SAM).[44]

The next issue to be clarified is whether the PDOS of the mixed SAM is merely a superposition of the PDOSs of the two subsystems, that is, a −CN and an $-NH_2$ substituted SAM at half coverage. This is necessary because it has been shown in ref 43 that, upon reducing the SAM coverage, the energetic difference between the HOPS peaks of −CN and $-NH_2$ substituted SAMs increases. This effect is not unexpected considering that in the limiting case of an "infinitely" dilute monolayer one ought to arrive at the "isolated molecule" situation and the energy levels of isolated donor- and acceptor-substituted molecules clearly differ from each other. We find, however, that such effects become relevant only at coverages well below 0.5 (the coverage of the individual subsystems of the mixed SAM). This is indicated by the thin vertical lines in Figure 2 that show the respective HOPS peaks for the half-coverage SAMs at −0.74 eV ($-NH_2$) and −0.85 eV (−CN), respectively;[85] that is, coverage-dependent shifts contribute only about 25% to the overall peak splitting observed in the mixed monolayer.

The homogeneous half- and full-coverage systems will serve as reference systems for the remainder of this article. This is useful since the comparison allows strictly distinguishing between effects that can be observed already in the homogeneous subsystems (like coverage-dependent depolarization[43]) and such that arise from specific interaction of the two SAM components and, thus, go beyond a mere superposition of the properties of the subsystems.

SAMs in the Absence of the Metallic Substrate. At this point the question arises, which kind of interaction between the monolayer constituents is responsible for the unexpected electronic structure of the mixed SAM. To disentangle contributions from molecule/molecule and metal/molecule interactions, we discuss the hypothetical situation of a free-standing SAM next. This system is realized by removing the metal slab and saturating the thiolates with hydrogen atoms.[44]

As the left-sided vacuum level is most relevant for the alignment of the SAM states with the metal Fermi energy (*cf.*, Figure 1c and corresponding discussion), the DOS of the different free-standing SAMs is best aligned at E_v^{left}, that is, the vacuum level at the side of the SAM that approaches the metal upon adsorption. The results for the mixed monolayer and the $-NH_2$ and −CN substituted biphenylthiolates at full coverage are shown as thick solid lines in the respective panels of Figure 3. As the two molecules in the surface unit cell are not symmetry equivalent even in the homogeneous SAMs, it is useful to partition the total DOS of the layer into the contributions of the two symmetry-inequivalent subsystems. The results are indicated as dark gray and crossed light gray areas. We find that (i) in the homogeneous layers, the inequivalence of the two molecules in the surface unit cell is essentially irrelevant for their level alignment; (ii) both, for the homogeneous $-NH_2$ and −CN substituted SAMs, the HOPS peak is found at approximately −5.1 eV; that is, also in the free-standing layers the tail-group substituent has almost no impact on the position of the HOPS relative to E_v^{left};[44] (iii) in the mixed SAM (top panel), the splitting of the eigenstates is even more pronounced in the absence of the metallic substrate (*ca.* 0.7 eV instead of 0.4 eV). This is because the HOPS peaks associated with the $-NH_2$ and −CN substituted molecules are shifted up by 0.43 eV and down by 0.23 eV compared to the homogeneous layers, as indicated by the dashed black arrows. The assignment of the various peaks to the different molecules is nicely confirmed by the insets, which show the local densities of states (corresponding to the charge density) within an energy window of 0.1 eV around the respective DOS peaks. Like for the adsorbed SAM, we have also calculated the DOS of the individual components of the mixed monolayer, that is, the free-standing −CN and $-NH_2$ SAMs at half-

coverage, in the absence of the respective other fragment. This allows discriminating the effects arising from interaction between the individual components from a mere superposition of their respective DOS. Like in Figure 2, the resulting HOPS-peak positions are plotted as vertical lines in the topmost panel. They essentially coincide. This comparison clearly shows that the contribution of packing-density effects to the level splitting vanishes in the absence of the metallic substrate.

Explaining the Electronic Structure of Mixed Monolayers. ***Electrostatics.*** The above results allow the conclusion that the qualitative differences between homogeneous and mixed monolayers are due to molecule/molecule interactions. The interaction with the metal plays a mitigating role, as upon adsorption the splitting between the HOPS states of the $-NH_2$ and $-CN$ substituted subsystems is reduced to about half (*cf.*, Figures 2 and 3). A significant contribution to the intermolecular interaction between polar molecules is electrostatic. To elucidate the role of such electrostatic interactions, we have calculated the potential energies for an electron in the two subsystems ($-NH_2$ and $-CN$ substituted monolayers at half coverage), $E_{NH2\text{-}1/2'}$ and $E_{CN\text{-}1/2''}$. Prime and double prime denote the two inequivalent sites for the molecules in the unit cell. The results are shown in Figure 4a for a few neighboring cells averaged along the *x*-axis of the unit cell (*cf.* Figure 1). Isodensity lines spaced by 0.1 eV clearly show that, compared to the common zero defined as the energy of the "left" vacuum level, the electrostatic energy in the region between the molecules decreases continuously for the $-NH_2$ substituted biphenylthiols, while it increases for the $-CN$ substituted molecules. This region between the molecules at half coverage is where the additional molecules will be located in a densely packed SAM. Therefore, when going from half to full coverage, the additional molecules are embedded in the electrostatic energy landscape of the same type of molecules in a homogeneous monolayer, while they feel the electrostatic energy landscape of the other type of molecules in a mixed monolayer. In the latter case, this shifts the eigenstates of the $-NH_2$ substituted molecules up in energy and those of the $-CN$ substituted molecules down, resulting in the peculiar level alignment discussed above.[86] This mechanism is schematically summarized in Figure 4b, where the electrostatic potential energy landscape is sketched for the half-coverage SAMs with the tail-group dipole moments pointing toward the right (1a) and toward the left (1b), respectively. Their HOPS levels are drawn as gray (green) bars. Panel 2 shows the changes in potential energy that affect the molecules in subsystems 1a and 1b upon merging. I.e., it schematically combines the electrostatic potential energy arising from the $-CN$ substituted sub-system at the position where the $-NH_2$ substituted molecules are found in the mixed SAM and vice versa. The energy levels of the molecules are modified

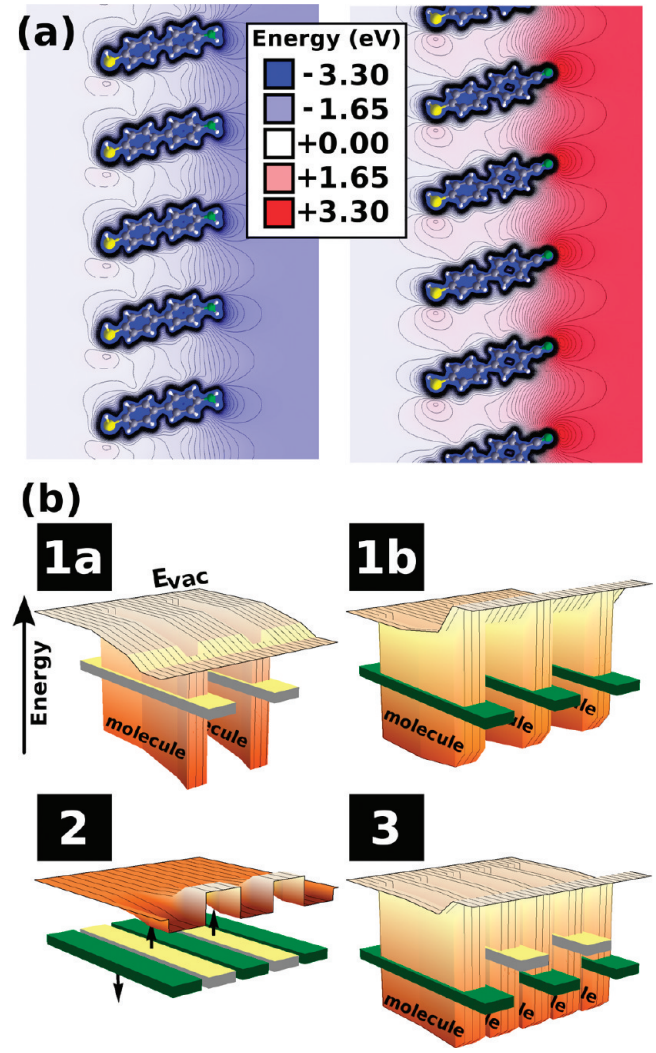

Figure 4. (a) Electrostatic energies $E_{NH_2\text{-}1/2'}$ (left) and $E_{CN\text{-}1/2''}$ (right) across the components of the mixed monolayer. The plots are averaged along the *x*-axis of the unit cell (*cf.* Figure 1) and aligned at E_v^{left}; the unit of energy is eV and isolines are drawn every 0.1 eV. (b) Schematic illustration of the electrostatic situation in mixed SAMs. Panels a and b show the potential energy landscape in the two subsystems before mixing. HOPS levels are drawn as gray (green) bars. Panel 2 shows the changes in potential energy that affect the molecules in the subsystems upon mixing and how those changes shift their eigenstates. The situation after mixing is shown in panel 3.

accordingly: The HOPS of molecules belonging to subsystem 1a are shifted up and states in subsystem 1b are shifted down in energy. This results in the situation shown in panel 3. We note that, because of the nature of this effect, a prerequisite for an experimental confirmation of the predicted level-splitting by ultraviolet photoelectron spectroscopy (UPS) measurements is a mixing of the differently substituted molecules at the molecular scale.

Polarization and Depolarization. Following the same line of argument for the respective homogeneous layers, this explanation implies a corresponding downward (upward) shift of the eigenvalues for the homogeneous $-NH_2$ ($-CN$) substituted layers upon increasing the packing density from half to full coverage. Hence, it

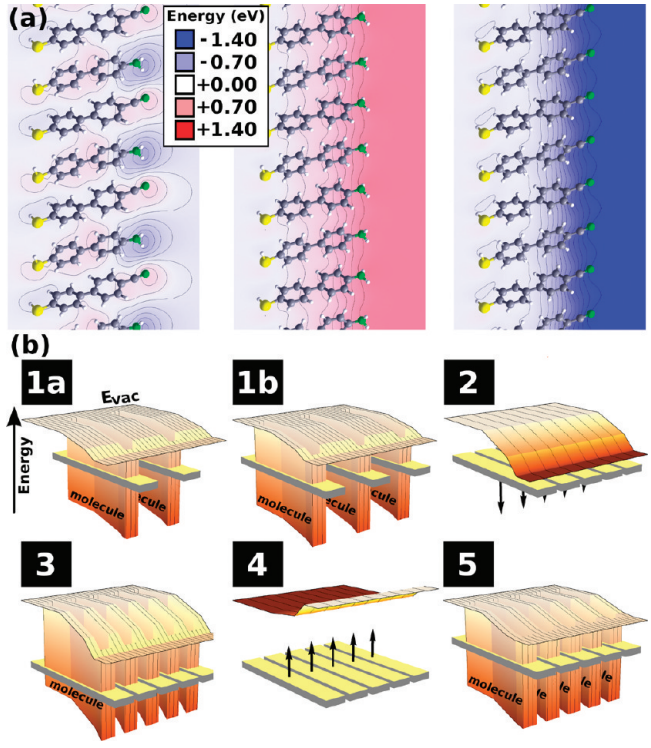

Figure 5. (a) Effect of (de)polarization on the electron electrostatic energy ΔE_{mixed} (left), ΔE_{NH_2} (center), and ΔE_{CN} (right) when combing the components of the mixed SAM (left) and when doubling the packing density of the respective pure layers from half to full coverage (center and right). See text for the definition of these quantities. The energies are averaged along the *x*-axis of the unit cell (*cf.* Figure 1) and isolines are drawn every 0.1 eV. (b) Sketch of the electrostatic energy landscape for increasing the packing density of a homogeneous $-NH_2$ SAM from half to full coverage. Similar to Figure 4b, panels a and b show the potential energy landscape in the two subsystems before mixing; HOPS levels of $-NH_2$ substituted molecules are drawn as gray bars. Panel 2 shows the changes in potential energy that affect the molecules in the two subsystems upon mixing and how those changes shift their respective HOPS. The situation after mixing but prior to depolarization is shown in panel 3. Panel 4 shows the changes in potential energy which affect the molecules in the subsystems due to depolarization effects. The final situation (panel 5) differs from the mere electrostatic sum of the two half-coverage SAMs shown in panel 3.

seemingly contradicts the findings discussed above, which show that such shifts do virtually not occur between half and full coverage in the free-standing monolayer (*cf.* Figure 3). The reason for this is that the arguments in the Electrostatics subsection do not yet account for a second effect: When two half-coverage monolayers are merged to a full-coverage layer, the field originating from molecules in one half influences the molecules in the respective other half of the layer by depolarization or polarization.

Depolarization is a well-known effect in SAMs[39−43,83,84] and is a consequence of the fact that the electron cloud of every molecule within the SAM is polarized by the electric field that is the superposition of the fields generated by all other molecules in the SAM. In homogeneous layers, this field induces a dipole that points in the direction opposite to the intrinsic dipole of the molecule, thus reducing its dipole moment. Depolarization can be very large, especially for SAMs with highly polarizable backbones.[38] In a mixed monolayer, the opposite effect is to be expected. The antiparallel orientation of neighboring dipoles within the SAM leads to a mutual polarization giving rise to increased dipole moments.

To quantify the polarization and depolarization effects, we have plotted the DFT-calculated changes in the electrostatic energy that result from the interaction between two half-coverage subsystems in Figure 5a. The leftmost plot shows the difference in the electrostatic energy between the mixed monolayer, E_{mixed}, and the respective sublattices, $\Delta E_{mixed} = E_{mixed} - (E_{NH_2\text{-}1/2'} + E_{CN\text{-}1/2''})$. The central and rightmost plots show the equivalent quantities for the homogeneous $-NH_2$ and $-CN$ substituted SAMs when going from half to full coverage; these are defined as $\Delta E_{NH_2} = E_{NH_2} - (E_{NH_2\text{-}1/2'} + E_{NH_2\text{-}1/2''})$ and $\Delta E_{CN} = E_{CN} - (E_{CN\text{-}1/2'} + E_{CN\text{-}1/2''})$, respectively.

The main observations in Figure 5a are that (i), the sign of ΔE_{mixed} alternates between neighboring molecules as well as within each molecule; (ii) the most pronounced changes in energy are confined to the vicinity of the tail-group substituents. The energy decreases by up to 0.5 eV near the $-NH_2$ substituents while the increase near the $-CN$ groups is only up to 0.2 eV, consistent with the fact that the field at the locations of the $-NH_2$ groups (due to the $-CN$ dipoles) is much larger than the field in the spatial region of the $-CN$ groups (caused by $-NH_2$ dipoles; *cf.* also Figure 4a). (iii) Overall, those effects largely cancel: the change in electrostatic energy decreases only by 0.1 eV across the mixed SAM. (iv) No such cancellation is found in the homogeneous case. The signs of ΔE_{NH_2} and ΔE_{CN} are opposite but remain unchanged throughout the whole monolayer, resulting in sizable overall changes of +0.7 eV (for $-NH_2$) and −1.3 eV (for $-CN$) due to depolarization effects. In sharp contrast to the mixed case, isolines are to a good approximation parallel and significant changes in the electrostatic energy are found in the spatial region encompassing the second phenyl ring and the tail-group. On the basis of these data it is perfectly plausible to assume that this change in electrostatic energy again shifts the HOPS energy in the respective homogeneous layers. The direction of that shift is such that it compensates for the shift discussed in the Electrostatics subsection, that is, up (down) for the $-NH_2$ ($-CN$) substituted subsystem. In other words, when going from half to full coverage in a homogeneous SAM, the shift of the orbital energies induced by the fields that arise from the electrostatic interaction between the two subsystems (the effect discussed in the Electrostatics subsection) is fully compensated by the consequence of depolarization. In analogy to the scheme for the mixed SAM (Figure 4b), a sketch of the mechanisms proposed for homogeneous layers is shown in Figure 5b. Panels 1−3 correspond to the purely electrostatic picture described already in Figure

4b for the mixed case. The non-negligible impact of depolarization on the HOPS energy is illustrated in panel 4, and panel 5 sketches the final energetic situation.

In the mixed case, because the sign of ΔE_{mixed} within each molecule changes and because the most pronounced changes in energy are restricted to the vicinity of the tail-group substituents, the net contribution of polarization to the shift of the HOPS energies can be expected to be only of minor importance (*i.e.*, an effect analogous to that sketched in panel 4 of Figure 5b does not occur). The inequivalence of the changes in electrostatic energy in homogeneous and mixed SAMs are caused by the equivalent, respectively, different signs of the (de)polarization induced charge rearrangements (see Supporting Information) that eventually determine the changes in electrostatic energy *via* the 3D Poisson equation.

To test the above explanations and to quantify potential oversimplifications in the purely electrostatics-based explanation provided in the previous section, the role of those (de)polarization effects on the resulting DOS have to be considered. This can be done by calculating the DOS of the mixed and homogeneous full-coverage SAMs in a non-selfconsistent (nscf) way. To that end, we fix the charge density of the full-coverage SAM artificially to the sum of the (self-consistent) charge densities calculated for the two subsystems. This prevents any changes of the charge density due to (de)polarization and thus allows an estimation of the relative importance of (de)polarization processes for the correct, self-consistently calculated DOS. For details on the nscf-calculations, see the Methods section. The resulting nscf-DOSs are drawn as dashed orange lines in the corresponding panels of Figure 3. For the mixed SAM, the nscf-DOS practically matches the self-consistently calculated one (solid black line). This is plausible in the light of observations (i) and (ii) made above when discussing Figure 5a and shows that the assumption of minor impact of polarization on the DOS is surprisingly well justified. For the homogeneous $-NH_2$ ($-CN$) substituted SAM, the nscf-DOS is shifted to lower (higher) energies, that is, the depolarization effects included only in the fully self-consistent calculations significantly impact the DOS (solid blue and red lines). In other words, our straightforward electrostatic model established in the Electrostatics subsection is indeed well-suited to rationalize the observations for the mixed SAM, while it fails for homogeneous layers, where depolarization effects have to be included.

The above considerations do not allow definitely excluding minor contributions from the exchange-correlation interaction between the two half-coverage subsystems of a full-coverage SAM, but they suggest the following semiquantitative picture for intramolecular interactions within SAMs and the resulting level alignment: Upon proceeding from half to full coverage, the electrostatic energy landscape created by the donor- (acceptor-)substituted subsystem (shown in Figure 4) decreases (increases) the eigenenergies of the molecules that occupy the second adsorption site in the surface unit cell. If the latter bear a different substituent, that is, if one is dealing with a mixed monolayer, the impact of (de)polarization is negligible and the positions of the HOPS in the two subsystems are largely determined by this potential energy landscape (*cf.* Figure 4b). As a consequence, a significant energetic splitting between the respective HOPS peaks is observed (*cf.* Figure 3, top panel). In a homogeneous SAM, the above-mentioned downward (upward) shift of the molecular states is largely compensated by the respective upward (downward) shifts due to depolarization (shown in Figure 5b). As a net effect, there is only a very small difference between the positions of the HOPS peaks upon going from half to full coverage[43] or when replacing donor by acceptor substituents in a homogeneous SAM[44] (*cf.*, Figure 3).

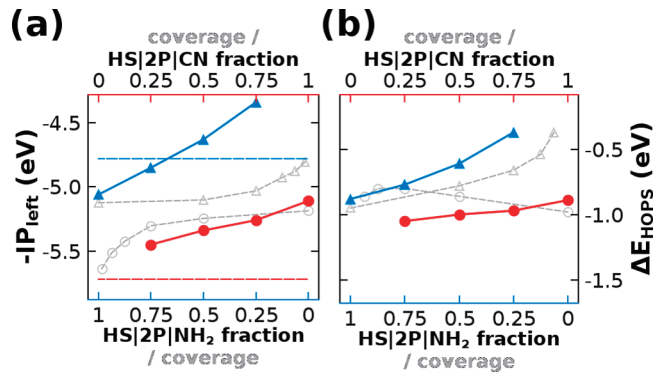

Figure 6. Energies of the HOMO-derived states with respect to the left vacuum energy E_v^{left} (a) and the metal Fermi energy (b) in the free-standing (a) and adsorbed (b) mixed monolayers, respectively. Blue triangles (red circles) show data for the amino- (cyano-)substituted component. Open gray triangles and circles depict the same quantities as a function of the packing density (rather than fraction), reproduced from ref 43. The dash−dotted horizontal blue (red) line in panel a shows the HOMO energy for the isolated amino- (cyano-)substituted biphenylthiol molecule (taken from Figure 3 in ref 43). The widths of the energy windows in panels a and b are the same.

Impact of the Mixing Ratio. As a next step, we will discuss the impact of the mixing ratio. To that aim, we have studied a densely packed $-NH_2$ substituted SAM in which an increasing fraction of the $-NH_2$ substituents is replaced by $-CN$ groups in steps of 25%. In this way, mixing ratios of 1:0, 3:1, 1:1, 1:3, and 0:1 are realized (for details on the considered surface unit cells, see Methods section). We first present the results for the free-standing mixed SAMs. Figure 6a shows data for the HOPS positions associated with the $-NH_2$ ($-CN$) substituted subsystems as blue triangles (red circles). The IP^{left} values for homogeneous SAMs at the corresponding submonolayer coverages are also included as light gray, open symbols.[43] This again allows discriminating between packing-density related effects relevant for each subsystem separately and the interaction between the subsystems. We note that in ref 43, the molecular tilt angle was kept constant at its value at full coverage

for all lower packing densities. This procedure is useful for modeling and facilitates a comparison with the mixed systems of the present study. In a real-world experiment, however, geometry-induced effects of a changing molecular (and dipole moment) orientation are to be expected. Naturally, the two data sets should coincide at −CN fractions of 0 and 1. The reason for the minor deviations we find in Figure 6 between our new data (colored) and the data taken from ref 43 (gray) is that we have used a more sophisticated geometry-optimization scheme here (details in the Methods section); this, however, has no impact on the following discussion. Furthermore, the ionization potentials of the isolated molecules (also taken from ref 43) are indicated by horizontal dash−dotted lines.

Figure 6a shows that, for the mixed monolayer, the positions of the HOPS peaks associated with the two subsystems depend approximately linearly on the mixing ratio. The slope for the $-NH_2$ related HOPS peak is higher. Hence, both the absolute positions of the levels and their splitting depend on the mixing ratio. In other words, reading the plot from left to right corresponds to increasing the fraction of −CN substituted molecules mixed into the $-NH_2$ substituted SAM, which causes a pronounced upward shift of the HOPS of the latter. Mixing amino-terminated molecules into the −CN substituted SAM (*i.e.*, reading the plot from right to left) has the opposite effect on its HOPS levels, but with smaller magnitude than for the $-NH_2$ substituted molecules. This can be rationalized by the smaller change in the electrostatic energy landscape induced by the $-NH_2$ substituted SAM in the region of the −CN substituted molecules (*cf.* Figure 4). Note that (de)polarization effects are negligible only at a 1:1 mixing ratio, while for the 1:3 and 3:1 cases one has to expect a situation intermediate between 1:1 mixing and homogeneous films.

For the HOPS energies at submonolayer coverage (light gray symbols), qualitatively different evolutions are observed. This is not surprising as depolarization-related shifts have greater influence in those systems (*cf.* also the Polarization and Depolarization subsection). For the limit of zero coverage, IP^{left} converges toward the IP of the isolated molecule (horizontal dash−dotted lines), as they form the "natural" limit in homogeneous SAMs.[43] Interestingly, this does not apply to the position of the HOPS of the minority component in mixed SAMs upon approaching the homogeneous film limit (*cf.*, filled red and blue symbols). This is because these molecules are embedded into a polar medium (*i.e.*, a close-packed SAM) rather than in vacuum.

As deduced already from a comparison of Figures 2 and 3, the metal mitigates the above-described effects to a certain extent. Figure 6b shows the energetic offset ΔE_{HOPS} between the metal Fermi level and the highest occupied π-states after adsorption. Light gray data points for reduced coverages are again reproduced from ref 43. While for the coverage-dependent calculations on homogeneous SAMs there are significant differences between the trends depicted in Figure 6a and Figure 6b, for the mixed monolayers only the magnitude of the splitting changes and the slope of the evolution of ΔE_{HOPS} with the mixing ratio is smaller than that of IP^{left} for both SAM components. For homogeneous SAMs, the substantial changes in the evolutions induced by the bonding to the metal can be unambiguously associated with a depolarization of the bonding-induced charge transfer at the metal−thiolate bond, that is, a reduced bond dipole at higher coverages.[43] In contrast, such effects do not occur in the mixed monolayers as changing the mixing ratio has no impact on the density of the thiolate groups on the surface. Moreover, it has been shown that in densely packed SAMs tail-group substitution hardly affects the bonding-induced charge rearrangements at the gold/molecule interface.[44] As a consequence, the bond dipole, which, besides IP^{left}, is the main quantity determining ΔE_{HOPS}[36], hardly changes with the mixing ratio.

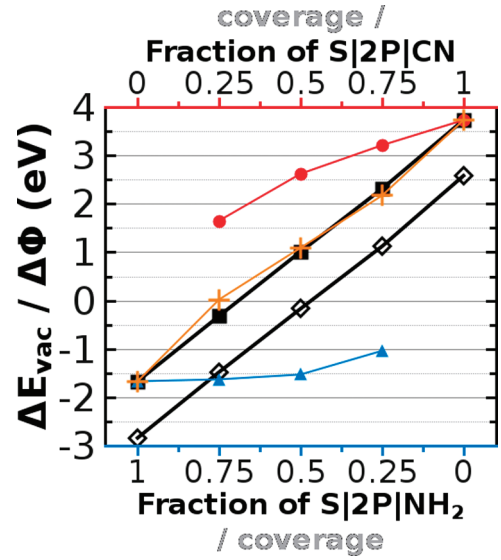

Figure 7. Change of the electron electrostatic energy, ΔE_{vac}, across the free-standing mixed SAM as a function of the mixing ratio (black squares), ΔE_{vac} across the mixed components in absence of the respective other fragment (blue triangles, $-NH_2$; red circles, −CN substituted component), their sum (orange crosses), and the SAM-induced work-function modification, $\Delta\Phi$, (open black diamonds). Note that per definition the impact of the bond-dipole, ΔE_{BD}, is given by $\Delta E_{BD} = \Delta\Phi - \Delta E_{vac}$.

SAM-Induced Work-Function Changes in Mixed Monolayers. Understanding the bond dipole in mixed monolayers is an important prerequisite for analyzing the second key electronic parameter of SAMs on metal surfaces, namely the SAM-induced work-function modification, $\Delta\Phi$. The latter can be conveniently understood as the sum of the vacuum-level shift between the "left" and "right" sides of the free-standing monolayer (*cf.* Figure 1c) denoted as ΔE_{vac} and a second step in the electrostatic potential energy due to the bond dipole, ΔE_{BD}.[33,44] The DFT-calculated ΔE_{vac} and $\Delta\Phi$ are shown as black,

solid squares and black, open diamonds in Figure 7. With respect to ΔE_{vac}, $\Delta\Phi$ is more or less rigidly shifted to more negative energies by $\Delta E_{BD} = -1.17 \pm 0.03$ eV. On the one hand, this confirms that the bond dipole is independent of the SAM composition. On the other hand, it underlines that the key to understanding the evolution of $\Delta\Phi$ with the SAM mixing ratio is understanding the evolution of ΔE_{vac}, that is, the property of the free-standing monolayer.

Both ΔE_{vac} and $\Delta\Phi$ display a close to linear evolution with the $-NH_2$ to $-CN$ ratio. For the related system of alkanethiols mixed with fluorinated alkanethiols on a silver surface this linear dependence was also experimentally observed for $\Delta\Phi$.[52] At a first glance, this might appear somewhat surprising, considering that $\Delta\Phi$ and ΔE_{vac} have been shown to increase in a strongly sublinear fashion with coverage in homogeneous SAMs due to depolarization effects.[84,43] Such a behavior is observed also here, when calculating only the homogeneous subsystems corresponding to 25%, 50%, 75%, and 100% coverage shown as red circles and blue triangles in Figure 7. The sublinearity in the coverage is particularly pronounced for the $-NH_2$ substituted SAM, where ΔE_{vac} increases only from -1.04 to -1.67 eV between 25% and full coverage.

Nevertheless, the trend for the mixed system should then, to a first approximation, be recovered by a simple addition of the contributions of the individual subsystems, as ΔE_{vac} is essentially an "electrostatic" quantity. The results of such an addition are shown as orange crosses in Figure 7. Especially at half coverage, this procedure yields a value virtually identical to the fully self-consistently calculated one (black squares). This is not unexpected, considering the only very weak polarization effects resulting in an almost vanishing ΔE_{mixed} when combining the two half-coverage systems to a 1:1 mixed monolayer (see discussion of Figure 5). For the 3:1 and 1:3 mixing ratios the self-consistent values are slightly shifted in the direction of the minority component, indicating that the latter is impacted by polarization effects to a somewhat larger extent.

From a practical point of view, the main conclusion that can be drawn from Figure 7 is that, if one is able to fabricate a molecular-level mixed SAM, this opens up a way for tuning substrate work-functions over a much wider range than would be possible by changing the coverage using only a single component, where one is limited by depolarization effects. Finally, the linearity of all important SAM properties with the mixing ratio (*cf.*, Figure 6 and Figure 7) significantly facilitates the prediction of the interfacial properties.

CONCLUSIONS

We investigated molecular-level mixed SAMs of donor- and acceptor-substituted biphenylthiolates on the Au(111) surface by means of slab-type DFT calculations. We find a splitting of the electronic states associated with the SAM components in contrast to the respective pristine layers, where the end-group substitution has no impact on the alignment of the highest occupied π-state relative to the metal Fermi level. This shows that the electronic structure of molecularly mixed SAMs differs significantly from the mere superposition of its components. The differences can be rationalized by the electrostatic interaction between the sublattices of the mixed-SAM components. Polarization and depolarization effects are shown to play virtually no role for the level alignment in a mixed SAM at 1:1 mixing ratio. We furthermore show that the mixing-ratio dependences of the quantities of interest for applications, namely band alignment and work-function modification, show qualitatively entirely different evolutions than they do as a function of coverage in homogeneous SAMs. In particular, the strongly sublinear dependence on the coverage due to pronounced depolarization is absent in mixed SAMs. This results in an almost perfectly linear relationship between the work-function change as well as the level alignment and the mixing ratio in heterogeneous SAMs.

METHODS

The density-functional theory calculations were performed using the VASP code.[87] Valence electrons were described by a plane-wave basis set (kinetic energy cutoff of approximately 20 Ry) and valence−core electron interactions by the projector augmented-wave (PAW) method.[88,89] $8 \times 5 \times 1$ and $4 \times 5 \times 1$ Monkhorst−Pack[90] *k*-point grids were chosen for the 1:0, 1:1, 0:1, and for the 3:1 and 1:3 mixing ratios, respectively. A Methfessel−Paxton occupation scheme with a broadening of 0.2 eV was used. Geometry optimizations were performed using nonredundant internal coordinates based on the DIIS (direct inversion in the iterative subspace) method as implemented in the GADGET tool.[91] This approach is clearly superior to optimization in Cartesian coordinates for systems like those studied here. Ionic relaxations were stopped as soon as every force component fell below 0.01 eV/Å. For electronic relaxations, two separate convergence criteria were applied: a total energy change $\Delta E < 1 \times 10^{-4}$ eV and a step in the electrostatic energy (which is proportional to the dipole moment per area) of 0.01 eV. The metal was modeled by five layers of Au(111) atoms and the resulting unit cell was periodically repeated in all three directions. To exclude spurious interactions between subsequent slabs, a vacuum gap of >20 Å was introduced in the *z*-direction together with a dipole layer within that vacuum gap to compensate for the asymmetry of the slab. During geometry relaxations, the coordinates of the lower three gold layers were fixed (representing the bulk), while the upper two layers (representing the surface) were free to move. Mixing ratios of 3:1 and 1:3 were realized by doubling the length of the shorter lattice vector pointing along the *x*-axis, thus obtaining surface unit cells comprising four molecules (the respective surface unit cells are included in the Supporting Information). Finer steps would require prohibitively large unit cells; already for a ratio of 1:3 (3:1), unit cells comprising 4 molecules and 60 gold atoms are needed. After setting the

mixing ratio, the ionic positions were reoptimized. The free-standing SAMs were investigated in the geometry obtained by relaxation in the adsorbed state and the thiolates were saturated by hydrogen atoms. When summing up the charge densities of two subsystems to obtain the input density for a non-selfconsistent (nscf) calculation, the PAW occupancies were left unchanged at their values in the subsystems. We note that, strictly speaking, the nscf-DOS cannot be interpreted as the DOS in absence of polarization since, precisely because of the lack of self-consistency, the corresponding orbital energies are not eigenvalues of the Kohn−Sham Hamiltonian of the system. Rather, the applied procedure should be seen as a method of estimating the importance of (de)polarization on the energy levels. Projected densities of states were calculated using the projection scheme implemented in the VASP code for the PAW method, which is an approximation as an unambiguous partitioning is impossible. A consequence of this scheme is that, usually, the sum of the projections onto all sub-systems does not completely recover the full density of states (cf. Figure 3). Nevertheless, the qualitative picture is well preserved. Further details regarding the applied computational methodology and the used parameters are given in ref 79. Representations of the systems and the potential energy landscapes were generated using XCrysDen.[92]

Acknowledgment. We thank the ZID of the TU Graz for providing computational resources. Support by the FWF through project P20972-N20 is gratefully acknowledged. We thank Dr. T. Bučko for providing and acquainting us with the GADGET code and Dr. M. Marsman for his kind help concerning the non-selfconsistent calculations.

Supporting Information Available: Figures depicting the construction of the unit cell for mixing ratios other than 1:1 and showing the charge rearrangements in mixed and homogeneous monolayers caused by (de)polarization effects upon going from half to full coverage. This material is available free of charge *via* the Internet at http://pubs.acs.org.

REFERENCES AND NOTES

1. Ulman, A. Formation and Structure of Self-Assembled Monolayers. *Chem. Rev.* **1996**, *96*, 1533–1554.
2. Schreiber, F. Self-Assembled Monolayers: From Simple Model Systems to Biofunctionalized Interfaces. *J. Phys.: Condens. Matter* **2004**, *16*, R881–R900.
3. Kind, M.; Wöll, C. Organic Surfaces Exposed by Self-Assembled Organothiol Monolayers: Preparation, Characterization, and Application. *Prog. Surf. Sci.* **2009**, *84*, 230–278.
4. Love, J. C.; Estroff, L. A.; Kriebel, J. K.; Nuzzo, R. G.; Whitesides, G. M. Self-Assembled Monolayers of Thiolates on Metals as a Form of Nanotechnology. *Chem. Rev.* **2005**, *105*, 1103–1170.
5. Gooding, J.; Mearns, F.; Yang, W.; Liu, J. Self-Assembled Monolayers into the 21st Century: Recent Advances and Applications. *Electroanalysis* **2003**, *15*, 81–96.
6. Fontaine, P.; Goguenheim, D.; Deresmes, D.; Vuillaume, D.; Garet, M.; Rondelez, F. Octadecyltrichlorosilane Monolayers as Ultrathin Gate Insulating Films in Metal−Insulator−Semiconductor Devices. *Appl. Phys. Lett.* **1993**, *62*, 2256–2258.
7. Guo, X.; Myers, M.; Xiao, S.; Lefenfeld, M.; Steiner, R.; Tulevski, G. S.; Tang, J.; Baumert, J.; Leibfarth, F.; Yardley, J. T.; Steigerwald, M. L.; Kim, P.; Nuckolls, C. Chemoresponsive Monolayer Transistors. *Proc. Natl. Acad. Sci. U.S.A.* **2006**, *103*, 11452–11456.
8. Bock, C.; Pham, D. V.; Kunze, U.; Kaäfer, D.; Witte, G.; Woäll, C. Improved Morphology and Charge Carrier Injection in Pentacene Field-Effect Transistors with Thiol-Treated Electrodes. *J. Appl. Phys.* **2006**, *100*, 114517.
9. Pacher, P.; Lex, A.; Proschek, V.; Etschmaier, H.; Tchernychova, E.; Sezen, M.; Scherf, U.; Grogger, W.; Trimmel, G.; Slugovc, C.; Zojer, E. Chemical Control of Local Doping in Organic Thin-Film Transistors: From Depletion to Enhancement. *Adv. Mater.* **2008**, *20*, 3143–3148.
10. Campbell, I. H.; Kress, J. D.; Martin, R. L.; Smith, D. L.; Barashkov, N. N.; Ferraris, J. P. Controlling Charge Injection in Organic Electronic Devices Using Self-Assembled Monolayers. *Appl. Phys. Lett.* **1997**, *71*, 3528–3530.
11. Yan, H.; Huang, Q.; Cui, J.; Veinot, J.; Kern, M.; Marks, T. High-Brightness Blue Light-Emitting Polymer Diodes *via* Anode Modification Using a Self-Assembled Monolayer. *Adv. Mater.* **2003**, *15*, 835–838.
12. de Boer, B.; Hadipour, A.; Mandoc, M. M.; van Woudenbergh, T.; Blom, P. W. M. Tuning of Metal Work Functions with Self-Assembled Monolayers. *Adv. Mater.* **2005**, *17*, 621–625.
13. Asadi, K.; Gholamrezaie, F.; Smits, E. C. P.; Blom, P. W. M.; Boer, B. D. Manipulation of Charge Carrier Injection into Organic Field-Effect Transistors by Self-Assembled Monolayers of Alkanethiols. *J. Mater. Chem.* **2007**, *17*, 1947–1953.
14. Ishii, H.; Sugiyama, K.; Ito, E.; Seki, K. Energy Level Alignment and Interfacial Electronic Structures at Organic/Metal and Organic/Organic Interfaces. *Adv. Mater.* **1999**, *11*, 605–625.
15. Koch, N. Energy Levels at Interfaces Between Metals and Conjugated Organic Molecules. *J. Phys.: Condens. Matter* **2008**, *20*, 184008.
16. Koch, N. Organic Electronic Devices and Their Functional Interfaces. *ChemPhysChem* **2007**, *8*, 1438–1455.
17. Chen, J.; Reed, M. A.; Rawlett, A. M.; Tour, J. M. Large On−Off Ratios and Negative Differential Resistance in a Molecular Electronic Device. *Science* **1999**, *286*, 1550–1552.
18. Kushmerick, J.; Holt, D.; Yang, J.; Naciri, J.; Moore, M.; Shashidhar, R. Metal−Molecule Contacts and Charge Transport Across Monomolecular Layers: Measurement and Theory. *Phys. Rev. Lett.* **2002**, *89*, 086802.
19. Akkerman, H. B.; Blom, P. W. M.; de Leeuw, D. M.; de Boer, B. Towards Molecular Electronics with Large-Area Molecular Junctions. *Nature* **2006**, *441*, 69–72.
20. Pace, G.; Ferri, V.; Grave, C.; Elbing, M.; von Hanisch, C.; Zharnikov, M.; Mayor, M.; Rampi, M. A.; Samori, P. Cooperative Light-Induced Molecular Movements of Highly Ordered Azobenzene Self-Assembled Monolayers. *Proc. Natl. Acad. Sci. U.S.A.* **2007**, *104*, 9937–9942.
21. Bumm, L. A.; Arnold, J. J.; Cygan, M. T.; Dunbar, T. D.; Burgin, T. P.; Jones, L.; Allara, D. L.; Tour, J. M.; Weiss, P. S. Are Single Molecular Wires Conducting. *Science* **1996**, *271*, 1705–1707.
22. Reed, M. A.; Zhou, C.; Muller, C. J.; Burgin, T. P.; Tour, J. M. Conductance of a Molecular Junction. *Science* **1997**, *278*, 252–254.
23. Donhauser, Z. J.; Mantooth, B. A.; Kelly, K. F.; Bumm, L. A.; Monnell, J. D.; Stapleton, J. J.; Price, D. W., Jr.; Rawlett, A. M.; Allara, D. L.; Tour, J. M.; Weiss, P. S. Conductance Switching in Single Molecules Through Conformational Changes. *Science* **2001**, *292*, 2303–2307.
24. Park, J.; Pasupathy, A. N.; Goldsmith, J. I.; Chang, C.; Yaish, Y.; Petta, J. R.; Rinkoski, M.; Sethna, J. P.; Abruña, H. D.; McEuen, P. L.; Ralph, D. C. Coulomb Blockade and the Kondo Effect in Single-Atom Transistors. *Nature* **2002**, *417*, 722–725.
25. Nitzan, A.; Ratner, M. A. Electron Transport in Molecular Wire Junctions. *Science* **2003**, *300*, 1384–1389.
26. Xu, B.; Tao, N. J. Measurement of Single-Molecule Resistance by Repeated Formation of Molecular Junctions. *Science* **2003**, *301*, 1221–1223.
27. Lörtscher, E.; Ciszek, J.; Tour, J.; Riel, H. Reversible and Controllable Switching of a Single-Molecule Junction. *Small* **2006**, *2*, 973–977.
28. Venkataraman, L.; Klare, J. E.; Nuckolls, C.; Hybertsen, M. S.; Steigerwald, M. L. Dependence of Single-Molecule Junction Conductance on Molecular Conformation. *Nature* **2006**, *442*, 904–907.

29. Zehner, R. W.; Parsons, B. F.; Hsung, R. P.; Sita, L. R. Tuning the Work Function of Gold with Self-Assembled Monolayers Derived from X−[C_6H_4−C≡C−]$_n$$C_6H_4$−SH ($n$ = 0, 1, 2; X = H, F, CH_3, CF_3, and OCH_3). *Langmuir* **1999**, *15*, 1121–1127.
30. De Renzi, V.; Rousseau, R.; Marchetto, D.; Biagi, R.; Scandolo, S.; del Pennino, U. Metal Work-Function Changes Induced by Organic Adsorbates: A Combined Experimental and Theoretical Study. *Phys. Rev. Lett.* **2005**, *95*, 046804.
31. Sun, Q.; Selloni, A.; Scoles, G. Electronic Structure of Metal/Molecule//Metal Junctions: A Density Functional Theory Study of the Influence of the Molecular Terminal Group. *J. Phys. Chem. B* **2006**, *110*, 3493–3498.
32. Rusu, P.; Giovannetti, G.; Brocks, G. Dipole Formation at Interfaces of Alkanethiolate Self-assembled Monolayers and Ag(111). *J. Phys. Chem. C* **2007**, *111*, 14448–14456.
33. Heimel, G.; Romaner, L.; Zojer, E.; Bredas, J. The Interface Energetics of Self-Assembled Monolayers on Metals. *Acc. Chem. Res.* **2008**, *41*, 721–729.
34. De Renzi, V. Understanding the Electronic Properties of Molecule/Metal Junctions: The Case Study of Thiols on Gold. *Surf. Sci.* **2009**, *603*, 1518–1525.
35. Heimel, G.; Rissner, F.; Zojer, E. Modeling the Electronic Properties of π-Conjugated Self-Assembled Monolayers. *Adv. Mater.* **2010**, *22*, 2494–2513.
36. Heimel, G.; Romaner, L.; Zojer, E.; Brédas, J. Toward Control of the Metal−Organic Interfacial Electronic Structure in Molecular Electronics: A First-Principles Study on Self-Assembled Monolayers of π-Conjugated Molecules on Noble Metals. *Nano Lett.* **2007**, *7*, 932–940.
37. Wang, J.; Prodan, E.; Car, R.; Selloni, A. Band Alignment in Molecular Devices: Influence of Anchoring Group and Metal Work Function. *Phys. Rev. B* **2008**, *77*, 245443.
38. Wang, L.; Rangger, G. M.; Romaner, L.; Heimel, G.; Bučko, T.; Ma, Z.; Li, Q.; Shuai, Z.; Zojer, E. Electronic Structure of Self-Assembled Monolayers on Au(111) Surfaces: The Impact of Backbone Polarizability. *Adv. Funct. Mater.* **2009**, *19*, 3766–3775.
39. Natan, A.; Zidon, Y.; Shapira, Y.; Kronik, L. Cooperative Effects and Dipole Formation at Semiconductor and Self-Assembled-Monolayer Interfaces. *Phys. Rev. B* **2006**, *73*, 193310.
40. Cornil, D.; Olivier, Y.; Geskin, V.; Cornil, J. Depolarization Effects in Self-Assembled Monolayers: A Quantum-Chemical Insight. *Adv. Funct. Mater.* **2007**, *17*, 1143–1148.
41. Sushko, M. L.; Shluger, A. L. Intramolecular Dipole Coupling and Depolarization in Self-Assembled Monolayers. *Adv. Funct. Mater.* **2008**, *18*, 2228–2236.
42. Romaner, L.; Heimel, G.; Ambrosch-Draxl, C.; Zojer, E. The Dielectric Constant of Self-Assembled Monolayers. *Adv. Funct. Mater.* **2008**, *18*, 3999–4006.
43. Romaner, L.; Heimel, G.; Zojer, E. Electronic Structure of Thiol-Bonded Self-Assembled Monolayers: Impact of Coverage. *Phys. Rev. B* **2008**, *77*, 045113.
44. Heimel, G.; Romaner, L.; Brédas, J.; Zojer, E. Interface Energetics and Level Alignment at Covalent Metal−Molecule Junctions: π-Conjugated Thiols on Gold. *Phys. Rev. Lett.* **2006**, *96*, 196806.
45. Bain, C. D.; Evall, J.; Whitesides, G. M. Formation of Monolayers by the Coadsorption of Thiols on Gold: Variation in the Head Group, Tail Group, and Solvent. *J. Am. Chem. Soc.* **1989**, *111*, 7155–7164.
46. Bain, C. D.; Whitesides, G. M. Formation of Monolayers by the Coadsorption of Thiols on Gold: Variation in the Length of the Alkyl Chain. *J. Am. Chem. Soc.* **1989**, *111*, 7164–7175.
47. Folkers, J. P.; Laibinis, P. E.; Whitesides, G. M. Self-Assembled Monolayers of Alkanethiols on Gold: Comparisons of Monolayers Containing Mixtures of Short- and Long-Chain Constituents with Methyl and Hydroxymethyl Terminal Groups. *Langmuir* **1992**, *8*, 1330–1341.
48. Bertilsson, L.; Liedberg, B. Infrared Study of Thiol Monolayer Assemblies on Gold: Preparation, Characterization, and Functionalization of Mixed Monolayers. *Langmuir* **1993**, *9*, 141–149.
49. Ballav, N.; Terfort, A.; Zharnikov, M. Mixing of Nonsubstituted and Partly Fluorinated Alkanethiols in a Binary Self-Assembled Monolayer. *J. Phys. Chem. C* **2009**, *113*, 3697–3706.
50. Kankate, L.; Turchanin, A.; Gölzhäuser, A. On the Release of Hydrogen from the S−H groups in the Formation of Self-Assembled Monolayers of Thiols. *Langmuir* **2009**, *25*, 10435–10438.
51. Silien, C.; Räisänen, M. T.; Buck, M. A Supramolecular Network as Sacrificial Mask for the Generation of a Nanopatterned Binary Self-Assembled Monolayer. *Small* **2010**, *6*, 391–394.
52. Wu, K.; Yu, S.; Tao, Y. Continuous Modulation of Electrode Work Function with Mixed Self-Assembled Monolayers and Its Effect in Charge Injection. *Langmuir* **2009**, *25*, 6232–6238.
53. Folkers, J. P.; Laibinis, P. E.; Whitesides, G. M.; Deutch, J. Phase Behavior of Two-Component Self-Assembled Monolayers of Alkanethiolates on Gold. *J. Phys. Chem.* **1994**, *98*, 563–571.
54. Chen, S.; Li, L.; Boozer, C. L.; Jiang, S. Controlled Chemical and Structural Properties of Mixed Self-Assembled Monolayers of Alkanethiols on Au(111). *Langmuir* **2000**, *16*, 9287–9293.
55. Chen, S.; Li, L.; Boozer, C. L.; Jiang, S. Controlled Chemical and Structural Properties of Mixed Self-Assembled Monolayers by Coadsorption of Symmetric and Asymmetric Disulfides on Au(111). *J. Phys. Chem. B* **2001**, *105*, 2975–2980.
56. Kang, J. F.; Ulman, A.; Liao, S.; Jordan, R. Mixed Self-Assembled Monolayers of Highly Polar Rigid Biphenyl Thiols. *Langmuir* **1999**, *15*, 2095–2098.
57. Kang, J. F.; Liao, S.; Jordan, R.; Ulman, A. Mixed Self-Assembled Monolayers of Rigid Biphenyl Thiols: Impact of Solvent and Dipole Moment. *J. Am. Chem. Soc.* **1998**, *120*, 9662–9667.
58. Ooi, Y.; Hobara, D.; Yamamoto, M.; Kakiuchi, T. Ideal Nonideality in Adsorption of 2-Aminoethanethiol and 2-Mercaptoethane Sulfonic Acid To Form Electrostatically Stabilized Binary Self-Assembled Monolayers on Au(111). *Langmuir* **2005**, *21*, 11185–11189.
59. Doneux, T.; De Decker, Y. A Simple Model to Describe the Effect of Electrostatic Interactions on the Composition of Mixed Self-Assembled Monolayers. *Langmuir* **2009**, *25*, 2199–2203.
60. Salaita, K.; Amarnath, A.; Maspoch, D.; Higgins, T. B.; Mirkin, C. A. Spontaneous "Phase Separation" of Patterned Binary Alkanethiol Mixtures. *J. Am. Chem. Soc.* **2005**, *127*, 11283–11287.
61. Ballav, N.; Weidner, T.; Röβler, K.; Lang, H.; Zharnikov, M. A New Approach for the Fabrication of Strongly Heterogeneous Mixed Self-Assembled Monolayers. *ChemPhysChem* **2007**, *8*, 819–822.
62. Ballav, N.; Shaporenko, A.; Krakert, S.; Terfort, A.; Zharnikov, M. Tuning the Exchange Reaction between a Self-Assembled Monolayer and Potential Substituents by Electron Irradiation. *J. Phys. Chem. C* **2007**, *111*, 7772–7782.
63. Troughton, E. B.; Bain, C. D.; Whitesides, G. M.; Nuzzo, R. G.; Allara, D. L.; Porter, M. D. Monolayer Films Pprepared by the Spontaneous Self-Assembly of Symmetrical and Unsymmetrical Dialkyl Sulfides from Solution onto Gold Substrates: Structure, Properties, and Reactivity of Constituent Functional Groups. *Langmuir* **1988**, *4*, 365–385.
64. Shon, Y.; Lee, S.; Perry, S. S.; Lee, T. R. The Adsorption of Unsymmetrical Spiroalkanedithiols onto Gold Affords Multicomponent Interfaces That Are Homogeneously Mixed at the Molecular Level. *J. Am. Chem. Soc.* **2000**, *122*, 1278–1281.
65. Shon, Y.; Lee, S.; Colorado, R.; Perry, S. S.; Lee, T. R. Spiroalkanedithiol-Based SAMs Reveal Unique Insight into the Wettabilities and Frictional Properties of Organic Thin Films. *J. Am. Chem. Soc.* **2000**, *122*, 7556–7563.

66. Heister, K.; Allara, D. L.; Bahnck, K.; Frey, S.; Zharnikov, M.; Grunze, M. Deviations from 1:1 Compositions in Self-Assembled Monolayers Formed from Adsorption of Asymmetric Dialkyl Disulfides on Gold. *Langmuir* **1999**, *15*, 5440–5443.
67. Madueno, R.; Räisänen, M. T.; Silien, C.; Buck, M. Functionalizing Hydrogen-Bonded Surface Networks with Self-Assembled Monolayers. *Nature* **2008**, *454*, 618–621.
68. Pace, G.; Petitjean, A.; Lalloz-Vogel, M.; Harrowfield, J.; Lehn, J.; Samorì, P. Subnanometer-Resolved Patterning of Bicomponent Self-Assembled Monolayers on Au(111). *Angew. Chem., Int. Ed.* **2008**, *47*, 2484–2488.
69. Salzmann, I.; Duhm, S.; Heimel, G.; Oehzelt, M.; Kniprath, R.; Johnson, R. L.; Rabe, J. P.; Koch, N. Tuning the Ionization Energy of Organic Semiconductor Films: The Role of Intramolecular Polar Bonds. *J. Am. Chem. Soc.* **2008**, *130*, 12870–12871.
70. Selzer, Y.; Cai, L.; Cabassi, M. A.; Yao, Y.; Tour, J. M.; Mayer, T. S.; Allara, D. L. Effect of Local Environment on Molecular Conduction: Isolated Molecule *versus* Self-Assembled Monolayer. *Nano Lett.* **2005**, *5*, 61–65.
71. Nottbohm, C. T.; Turchanin, A.; Gölzhäuser, A. Metallization of Organic Monolayers: Electroless Deposition of Cu onto Cross-Linked Aromatic Self-Assembled Monolayers. *Z. Phys. Chem.* **2008**, *222*, 917–926.
72. Al-Rawashdeh, N. A. F.; Azzam, W.; Wöll, C. Fabrication of an Amino-Terminated Organic Surface by Chemical Conversion of a Nitro-Terminated Self-Assembled Monolayer. *Z. Phys. Chem.* **2008**, *222*, 965–978.
73. Azzam, W.; Fuxen, C.; Birkner, A.; Rong, H.; Buck, M.; Wöll, C. Coexistence of Different Structural Phases in Thioaromatic Monolayers on Au(111). *Langmuir* **2003**, *19*, 4958–4968.
74. Weckenmann, U.; Mittler, S.; Naumann, K.; Fischer, R. A. Ordered Self-Assembled Monolayers of 4,4′-Biphenyldithiol on Polycrystalline Silver: Suppression of Multilayer Formation by Addition of Tri-*n*-butylphosphine. *Langmuir* **2002**, *18*, 5479–5486.
75. Liu, H.; Bhushan, B.; Eck, W.; Stadler, V. Investigation of the Adhesion, Friction, and Wear Properties of Biphenyl Thiol Self-Assembled Monolayers by Atomic Force Microscopy. *J. Vac. Sci. Technol. A* **2001**, *19*, 1234–1240.
76. Kleineberg, U.; Brechling, A.; Sundermann, M.; Heinzmann, U. STM Lithography in an Organic Self-Assembled Monolayer. *Adv. Funct. Mater.* **2001**, *11*, 208–212.
77. Leung, T.; Schwartz, P.; Scoles, G.; Schreiber, F.; Ulman, A. Structure and Growth of 4-Methyl-4′-mercaptobiphenyl Monolayers on Au(111): A Surface Diffraction Study. *Surf. Sci.* **2000**, *458*, 34–52.
78. Tao, Y.; Wu, C.; Eu, J.; Lin, W.; Wu, K.; Chen, C. Structure Evolution of Aromatic-Derivatized Thiol Monolayers on Evaporated Gold. *Langmuir* **1997**, *13*, 4018–4023.
79. Heimel, G.; Romaner, L.; Bredas, J.; Zojer, E. Organic/Metal Interfaces in Self-Assembled Monolayers of Conjugated Thiols: A First-Principles Benchmark Study. *Surf. Sci.* **2006**, *600*, 4548–4562.
80. Baker, K.; Fratini, A.; Resch, T.; Knachel, H.; Adams, W.; Socci, E.; Farmer, B. Crystal Structures, Phase Transitions and Energy Calculations of Poly(*p*-phenylene) Oligomers. *Polymer* **1993**, *34*, 1571–1587.
81. Vericat, C.; Vela, M. E.; Benitez, G.; Carro, P.; Salvarezza, R. C. Self-Assembled Monolayers of Thiols and Dithiols on Gold: New Challenges for a Well-Known System. *Chem. Soc. Rev.* **2010**, *39*, 1805–1834.
82. Natan, A.; Kronik, L.; Haick, H.; Tung, R. Electrostatic Properties of Ideal and Non-ideal Polar Organic Monolayers: Implications for Electronic Devices. *Adv. Mater.* **2007**, *19*, 4103–4117.
83. Gershevitz, O.; Sukenik, C. N.; Ghabboun, J.; Cahen, D. Molecular Monolayer-Mediated Control over Semiconductor Surfaces: Evidence for Molecular Depolarization of Silane Monolayers on Si/SiO_x. *J. Am. Chem. Soc.* **2003**, *125*, 4730–4731.
84. Fukagawa, H.; Yamane, H.; Kera, S.; Okudaira, K.; Ueno, N. Experimental Estimation of the Electric Dipole Moment and Polarizability of Titanyl Phthalocyanine Using Ultraviolet Photoelectron Spectroscopy. *Phys. Rev. B* **2006**, *73*, 041302(R).
85. The smaller (negative) values in both half-coverage systems compared to full coverage are a consequence of the coverage dependent bond dipole.[43] The slight differences in the peak positions compared to ref 43 (there values of −0.78 and −0.86 eV were found) are due to the improved geometry optimization scheme used in the present study.
86. At this point, it should be mentioned that the ionic relaxations we performed indicate that the mixed components interact also in terms of their geometry. For the donor headgroup $-NH_2$, two distinctly different conformations are possible. The plane of the pyramidal $-NH_2$ substituent can be oriented such that it reduces or increases the total molecular tilt angle with respect to the surface normal. For pure layers, both conformations are essentially equivalent in energy although they imply significantly different work-function modifications.[38] This changes in the mixed SAMs. Here, the geometry relaxes to the conformation in which a larger dipole moment perpendicular to the surface is associated with the $-NH_2$-substituted molecules so that they better compensate for the strong dipoles due to the −CN groups. This is consistent with the tendency of mixed SAMs to approach a situation with a net-dipole moment of zero as found experimentally.[56]
87. Kresse, G.; Furthmüller, J. Efficient Iterative Schemes for ab initio Total-Energy Calculations Using a Plane-Wave Basis Set. *Phys. Rev. B* **1996**, *54*, 11169–11186.
88. Blöchl, P. Projector Augmented-Wave Method. *Phys. Rev. B* **1994**, *50*, 17953–17979.
89. Kresse, G.; Joubert, D. From Ultrasoft Pseudopotentials to the Projector Augmented-Wave Method. *Phys. Rev. B* **1999**, *59*, 1758–1775.
90. Monkhorst, H.; Pack, J. Special Points for Brillouin-Zone Integrations. *Phys. Rev. B* **1976**, *13*, 5188–5192.
91. Bučko, T.; Hafner, J.; Ángyán, J. G. Geometry Optimization of Periodic Systems Using Internal Coordinates. *J. Chem. Phys.* **2005**, *122*, 124508.
92. Kokalj, A. Computer Graphics and Graphical User Interfaces as Tools in Simulations of Matter at the Atomic Scale. *Comput. Mater. Sci.* **2003**, *28*, 155–168, code available from http://www.xcrysden.org/.